Available online at www.sciencedirect.com
SCIENCE DIRECT®
Polyhedron 23 (2004) 2943–2954
POLYHEDRON
www.elsevier.com/locate/poly

Aromatic and aldehyde carbon–hydrogen bond activation at cationic Rh(III) centers. Evaluation of electronic substituent effects on aldehyde binding and C–H oxidative addition

Britton K. Corkey [a], Felicia L. Taw [a], Robert G. Bergman [b,*], Maurice Brookhart [a,*]

[a] Department of Chemistry, University of North Carolina at Chapel Hill, CB #3290, Chapel Hill, NC 27599-3290, USA
[b] Department of Chemistry, University of California and Division of Chemical Sciences, Lawrence Berkeley National Laboratory, Berkeley, CA 94720-1460, USA

Received 4 June 2004; accepted 2 September 2004
Available online 26 October 2004

Dedicated to Malcolm L.H. Green for his pathbreaking contributions to organometallic chemistry, his international collegiality, his wit, and his warmth

Abstract

Cationic rhodium methyl complexes, $[Cp^*(PMe_3)Rh(Me)(CH_2Cl_2)]BAr'_4$ (**1**) and $[Cp^*(P(OMe)_3)Rh(Me)(CH_2Cl_2)]BAr'_4$ (**3**), react with benzene to yield the corresponding phenyl complexes, $[Cp^*(PMe_3)Rh(Ph)(CH_2Cl_2)]BAr'_4$ (**6**) and $[Cp^*(P(OMe)_3)Rh(Ph)(CH_2Cl_2)]BAr'_4$ (**7**). First-order rate constants observed in 1.1 M benzene in CD_2Cl_2 at 25 °C are $(2.1 \pm 0.2) \times 10^{-5}$ s^{-1} and $(1.9 \pm 0.2) \times 10^{-5}$ s^{-1}, respectively. Reactions of **1** and **3** with *p*-X-substituted benzaldehydes (X = $-CF_3$, $-CH_3$, and –OMe) initially produce the σ-aldehyde adducts, $[Cp^*(L)Rh(Me)(p\text{-}XC_6H_4CHO)]BAr'_4$ (L = PMe_3 (**15**), $P(OMe)_3$ (**16**)). Exchange of free with bound aldehyde occurs via a dissociative process and quantitative NMR rate measurements show that complexes of **1** exchange faster than those of **3** and that less basic aldehydes exchange faster than more basic aldehydes (*p*-$CF_3C_6H_4CHO$ > *p*-$CH_3C_6H_4CHO$ > *p*-$CH_3OC_6H_4CHO$). The aldehyde adducts undergo C–H bond activation to produce initially methane plus acyl aldehyde adducts, $[Cp^*(L)Rh(C(O)C_6H_4X)(p - XC_6H_4CHO)]BAr'_4$ (L = PMe_3 (**17**), $P(OMe)_3$ (**18**)). Rates of C–H activation are correlated with aldehyde exchange rates; activation barriers of weakly bound aldehydes are lower than more strongly bound aldehydes. In the case of L = PMe_3, decarbonylation of the aldehyde adducts occurs cleanly to form aryl carbonyl complexes, $[Cp^*(PMe_3)Rh(C_6H_4X)(CO)]BAr'_4$. For L = $P(OMe)_3$, decarbonylation is a more complicated process; some intermediates and products have been identified by NMR spectroscopy.

Keywords: C–H bond activation; Rhodium(III); Benzene activation; Aldehyde activation

1. Introduction

Early examples of the oxidative addition reactions of alkane C–H bonds, leading to hydrido(alkyl)metal complexes, take place at metal centers in relatively low formal oxidation states. This has led to the general perception that electron-rich complexes are required in order to make this important oxidative addition process exergonic and therefore capable of generating stable products.

However, the platinum-based alkane functionalization reactions observed many years ago by Shilov and his coworkers [1], and the dehydrogenation

* Corresponding authors. Present address: Department of Chemistry, Los Alamos National Laboratory, Mailstop J514, Los Alamos, USA. Tel.: +1 505 6673968; fax: +1 505 6679905.
E-mail address: ftaw@lanl.gov (F.L. Taw).

0277-5387/$ - see front matter © 2004 Elsevier Ltd. All rights reserved.
doi:10.1016/j.poly.2004.09.005

reactions subsequently observed using high-valent iridium and rhenium complexes by the Crabtree [2] and Felkin [3] groups, were early indications that more electron-deficient metal centers could also undergo C–H oxidative addition. More recently, direct observation of C–H oxidative addition reactions at iridium (III) [4], as well as analogous reactions that take place in Pt(II) complexes [5], have made clear that such processes can occur at metal centers that are relatively electrophilic, and in some cases can be overall exergonic. This has given rise to a substantial increase in the number of studies directed toward alkane activation reactions involving higher-valent late transition metal complexes in recent years.

The cationic Ir(III) C–H oxidative addition reactions referred to above lead to relatively rare examples of organometallic positively-charged Ir(V) intermediates [6]. Many of these have been generated only in transient form, but a few have been found to be stable enough to isolate or detect in solution. In contrast to this growing body of research on Ir(III) C–H activation, much less attention has been directed toward the search for analogous reactions at Rh(III). In view of the fact that pentamethylcyclopentadienylrhodium(I) complexes were ultimately discovered to undergo C–H oxidative addition reactions analogous to those of their iridium congeners [7], we felt it would be interesting to look for Rh(III)-to-Rh(V) C–H oxidative addition reactions in related systems as well. This manuscript reports the results of our investigation of C–H bond activations of benzene and aryl aldehydes by $[Cp^*(L)Rh(Me)(CH_2Cl_2)]BAr'_4$ (L = PMe_3 (**1**), $P(OMe)_3$ (**3**)).

2. Results and discussion

2.1. Synthesis of cationic rhodium(III) methyl complexes, $[Cp^*(L)Rh(Me)(CH_2Cl_2)]BAr'_4$ (L = PMe_3 (**1**), $P(OMe)_3$ (**3**), Ar′ = 3,5-$(CF_3)_2C_6H_3$)

Synthesis of $[Cp^*(PMe_3)Rh(Me)(CH_2Cl_2)]BAr'_4$ (**1**) by treatment of Cp*(PMe_3)Rh(Me)(Cl) (**2**) with $NaBAr'_4$ has been previously reported by us [8]. This complex was fully characterized by NMR spectroscopy and X-ray diffraction studies. The phosphite analogue $[Cp^*(P(OMe)_3)Rh(Me)(CH_2Cl_2)]BAr'_4$ (**3**) was synthesized in a similar manner (Eq. (1)). The rhodium methyl chloride complex, Cp*($P(OMe)_3$)Rh(Me)(Cl) (**4**), was prepared by reaction of previously reported Cp*($P(OMe)_3$)$RhCl_2$ [9] with MeLi. The ^{1}H NMR spectrum of **3** in CD_2Cl_2 showed signals at 3.78 (d, $^3J_{P-H}$ = 11.4 Hz) for $P(OMe)_3$, 1.63 ppm (d, $^4J_{P-H}$ = 4.2 Hz) for Cp*, and 1.02 ppm (dd, $^3J_{P-H}$ = 5.5 Hz, $^2J_{Rh-H}$ = 1.5 Hz) for the Rh–CH_3 group. The $^{31}P\{^1H\}$ NMR signal appeared at 126.9 ppm (d, $^1J_{Rh-P}$ = 269 Hz), and the $^{13}C\{^1H\}$ NMR resonance of the Rh–CH_3 group exhibited a signal at 1.19 ppm (dd, $^2J_{P-C}$ = 37.1 Hz, $^1J_{Rh-C}$ = 22.0 Hz).

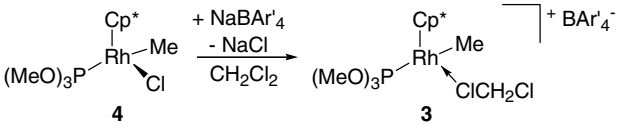

(1)

2.2. Carbon–hydrogen bond activation studies

In contrast to Bergman's cationic iridium (III) complex, $[Cp^*(PMe_3)Ir(Me)(CH_2Cl_2)]BAr'_4$ (**5**) [4b], the analogous rhodium methyl complex **1** does not react with alkanes to any appreciable extent, even at 45 °C. Addition of 500 equivalents of pentane to a CD_2Cl_2 solution of **1** resulted in the observation of only trace amounts of methane (by ^{1}H NMR) over the course of several days at 25 °C. Similar results were obtained with the corresponding Rh phosphite compound **3**. Given the inertness toward alkanes, studies of C–H bond activations using **1** and **3** focused on the more reactive substrates: benzene and aryl aldehydes.

2.3. Carbon–hydrogen bond activation of benzene

Rhodium methyl complexes **1** and **3** react with benzene to yield methane and the cationic rhodium phenyl complexes **6** and **7**, respectively (Eq. (2)). To further verify the structure of product **6**, this compound was independently synthesized and fully characterized by NMR spectroscopy and X-ray diffraction studies (see below). Product **7** was directly isolated from the C–H activation reaction of benzene and characterized by NMR spectroscopy.

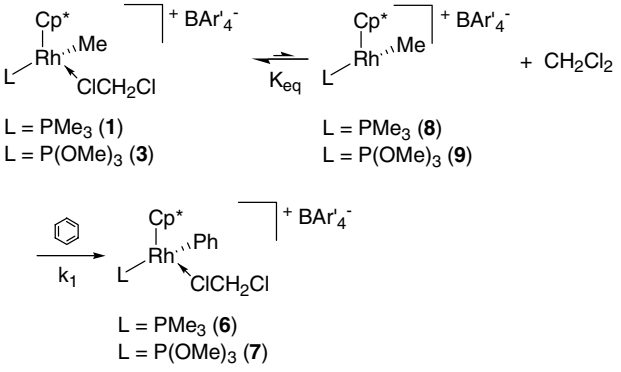

(2)

The rates of these reactions are sufficiently slow that clean conversions can be achieved only by using high ratios of benzene to rhodium complex. Under these conditions, the reactions exhibit clean pseudo-first order kinetics, as determined by integrations of ^{1}H NMR signals. Table 1 summarizes the observed first-order rate

Table 1
First-order rate constants for C–H activation of benzene by **1**, **3**, **5**, and **10**

$[Cp^*(L)M(Me)(CH_2Cl_2)]BAr'_4$	L = PMe_3	L = $P(OMe)_3$	Rate ratio
M = Rh[a]	$(2.1 \pm 0.2) \times 10^{-5}$ s^{-1}	$(1.9 \pm 0.2) \times 10^{-5}$ s^{-1}	(**1/3**) = 1.1
M = Ir[b]	$(8.4 \pm 0.8) \times 10^{-3}$ s^{-1}	$(3.0 \pm 0.3) \times 10^{-4}$ s^{-1}	(**5/10**) = 28.0

[a] 1.1 M C_6H_6 in CD_2Cl_2, 25 ± 2 °C.
[b] 0.26 M C_6H_6 in CD_2Cl_2, 0 °C.

constants for the reactions of **1** and **3** (0.02 M) with 1.1 M benzene in CD_2Cl_2 at 25 ± 2 °C. [1] For comparison, the reported rate constants [10] for the corresponding iridium analogues **5** and $[Cp^*(P(OMe)_3)Ir(Me)(CH_2Cl_2)]BAr'_4$ (**10**) reacting at 0 °C with 0.26 M benzene in CD_2Cl_2 are also listed.

In general, the iridium complexes **5** and **10** are far more reactive toward benzene than rhodium analogues **1** and **3**. Correcting for benzene concentrations, **5** reacts with benzene ca. 10^3 times faster than either **1** or **3** at a considerably lower temperature (0 °C vs. 25 °C). A significant feature of these comparisons is that, in the case of the Ir examples, the PMe_3 complex exhibits a rate ca. 30× that of the $P(OMe)_3$ complex; in contrast, the rates are comparable in the rhodium systems. Bergman has postulated that these reactions occur through the 16-electron species **11** and **12** (Eq. (3)) and that, while the presumably more electrophilic species **12** is expected to be more reactive (k_1 for $P(OMe)_3 > k_1$ for PMe_3), the value of K_{eq} for $P(OMe)_3$ is much less than K_{eq} for (PMe_3), resulting in $K_{eq(PMe_3)}k_{1(PMe_3)} > K_{eq(P(OMe)_3)}k_{1(P(OMe)_3)}$ [10]. In the case of the rhodium complexes, it appears that the $k_{1(PMe_3)} : k_{1(P(OMe)_3)}$ ratio is counterbalanced by the $K_{eq(P(OMe)_3)} : K_{eq(PMe_3)}$ ratio, and the observed rates of benzene activation are essentially equal (see Eq. (2)). The assumptions that Rh phosphite complex **9** is more electrophilic than the Rh phosphine complex **8** and that $K_{eq(PMe_3)} > K_{eq(P(OMe)_3)}$ receive independent support from observations described below in connection with the C–H bond activation of aryl aldehydes.

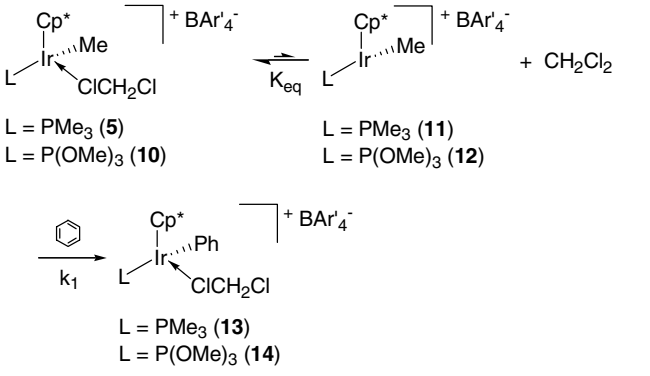

(3)

[1] Reactions of **1** and **3** in 2.2 M benzene in CD_2Cl_2 at 25 ± 2 °C give pseudo first-order rate constants of $(3.2 \pm 0.2) \times 10^{-5}$ s^{-1} and $(3.8 \pm 0.4) \times 10^{-5}$ s^{-1}, respectively. These data establish a clear dependence of the rate on benzene concentration.

2.4. Independent synthesis and characterization of $[Cp^*(PMe_3)Rh(Ph)(CH_2Cl_2)]BAr'_4$ (6)

To verify the identity of the product derived from C–H activation of benzene by rhodium methyl complex **1**, the cationic rhodium phenyl complex (**6**) was independently synthesized by adding $NaBAr'_4$ to a dichloromethane solution of previously reported $Cp^*(PMe_3)Rh(Ph)(Cl)$ [11]. X-ray quality, orange–red crystals of **6** were isolated in 70% yield. This compound is more thermally and air-sensitive than the rhodium methyl complex **1**, but can be stored under inert conditions at −30 °C for extended periods of time. An ORTEP diagram of **6** is shown in Fig. 1, with some selected bond distances and bond angles listed in Table 2. The bond distance between Rh and the ipso aryl carbon of the phenyl ring is 2.026(8) Å, which is shorter than the Rh–CH_3 bond length (2.106(5) Å) of complex **1** [8], as is expected for a metal bonded to an sp^2-hybridized carbon versus an sp^3 carbon. However, the Rh–Cl distance of phenyl complex **6** is 2.512(2) Å and differs only by 0.02 Å relative to the bond distance of 2.488(1) Å observed for the Rh–Cl bond of methyl complex **2** [8].

2.5. Carbon–hydrogen bond activation of aryl aldehydes

Bergman has shown that the iridium (III) complex $Cp^*(PMe_3)Ir(Me)(OTf)$ reacts rapidly with benzaldehyde at −80 °C to form an η^1-(O)-bound aldehyde

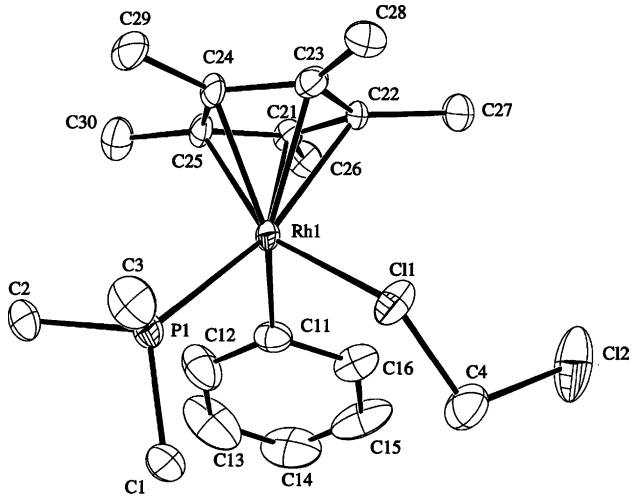

Fig. 1. ORTEP diagram of $[Cp^*(PMe_3)Rh(Ph)(CH_2Cl_2)]^+$ (**6**, BAr'_4^- counterion omitted for clarity).

Table 2
Selected bond distances and bond angles for complex **6**

	Bond distance (Å)		Bond angle (°)
Rh(1)–C(24)	2.195(6)	C(24)–Rh(1)–P(1)	101.5(2)
Rh(1)–P(1)	2.374(2)	C(11)–Rh(1)–Cl(1)	98.3(2)
Rh(1)–C(11)	2.026(8)	P(1)–Rh(1)–C(11)	87.9(3)
Rh(1)–Cl(1)	2.512(2)	P(1)–Rh(1)–Cl(1)	84.9(8)

adduct [12]. Upon warming to −60 °C, the adduct undergoes C–H bond activation and decarbonylation to form the iridium phenyl carbonyl complex, [Cp*(PMe_3)Ir(Ph)(CO)]OTf, and methane. Similarly, the cationic rhodium methyl complexes **1** and **3** react with aryl aldehydes (tolualdehyde, anisaldehyde, and 4-(trifluoromethyl)benzaldehyde) in CD_2Cl_2 at −80 °C to form η^1-aldehyde adducts (Eq. (4)).

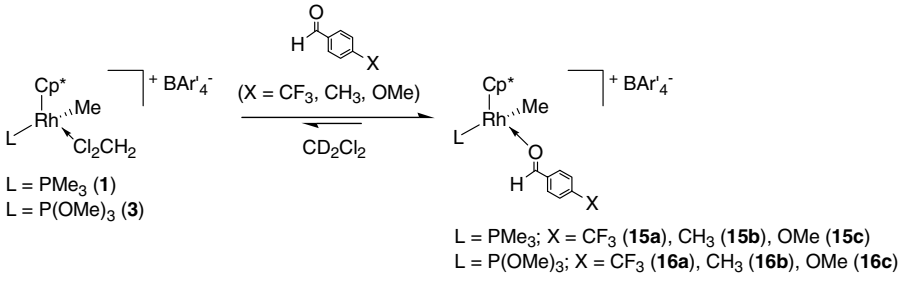

(4)

When reactions with **1** and **3** are carried out using excess aldehyde as substrate, ^{1}H NMR resonances for the aldehydic proton of both the bound and free aldehydes can be detected at low temperatures. The lack of rhodium coupling to the aldehydic hydrogen supports the η^1 structure. Upon warming, these resonances broaden and coalesce. The rates for loss of bound aldehydes from Rh were assessed by measuring the changes in line-width at half-height of the aldehydic protons and applying the slow exchange equation, $k = \pi(\Delta w)$. A key finding is that the linewidth and thus the rate of exchange of the bound aldehyde is *independent* of the concentration of free aldehyde. This clearly indicates the exchange occurs through a dissociative process. Table 3 summarizes the $\Delta G^{\ddagger}$ values obtained from line broadening experiments together with ^{1}H NMR shifts for free and bound aldehyde at −88 °C.

The trends follow the expected electronic effects. For both series **15a**–**15c** and **16a**–**16c** the order of dissociation is *p*-$CF_3C_6H_4CHO$ > *p*-$CH_3C_6H_4CHO$ > *p*-$CH_3OC_6H_4CHO$ which inversely parallels the order of basicity of the aldehydes. In comparing **15a**–**15c** with **16a**–**16c** in each of the three pairs the barrier to dissociation of aldehyde from the more electron-deficient $P(OMe)_3$ complex is ca. 1.7 kcal/mol higher than that for the more electron-rich PMe_3 complex. The strongest Rh(III)-aldehyde interaction is between the more electrophilic phosphite complex **16** and the most electron-rich aldehyde, *p*-$CH_3OC_6H_4CHO$. The weakest interaction is between the less electrophilic PMe_3 complex **15** and the most electron-deficient aldehyde, *p*-$CF_3C_6H_4CHO$.

The C–H activation chemistry of aryl aldehydes by rhodium complexes **1** and **3** is similar to the iridium chemistry but more complex in the case of **3**. Deinsertion products can react with **3** which complicates kinetic measurements and gives rise to a mixture of products. The most definitive kinetic studies were carried out using a large excess of aldehyde. First, this approach ensures that the equilibrium between the methylene chloride adducts **1** and **3** and the aldehyde adducts **15a**–**15c** and **16a**–**16c** lies strongly in favor of the aldehyde adducts. Second, and critical in the case of **3**, the C–H activation reactions result in generation of the Rh acyl aldehyde adducts **17** and **18**. Little deinsertion occurs under these conditions. The aldehyde adduct intermediate **15** or **16** builds up to high concentrations and clean first-order kinetics for conversion to **17** or **18**, respectively, are exhibited over ca. two half-lives (Eq. (5)). Rates and free energies of activation are summarized for these C–H bond activation reactions in Tables 4 and 5.

Table 3
Kinetic parameters for dissociation of bound aldehyde and ^{1}H NMR shifts (in ppm) for free and bound aldehyde at −88 °C

[Cp*(L)Rh(Me)(XC_6H_4CHO)]$^+$(η^1-aldehyde adduct)	k (s^{-1})	T (±2 °C)	$\Delta G^{\ddagger}$ (kcal/mol)	δ CHO (bound)	δ CHO (free)
L = PMe_3, X = CF_3 (**15a**)	50	−58	10.8 ± 0.1	9.38	10.02
L = PMe_3, X = CH_3 (**15b**)	60	−38	11.7 ± 0.2	9.13	9.87
L = PMe_3, X = OMe (**15c**)	75	−28	12.1 ± 0.2	8.97	9.79
L = $P(OMe)_3$, X = CF_3 (**16a**)	115	−18	12.4 ± 0.1	9.33	10.02
L = $P(OMe)_3$, X = CH_3 (**16b**)	105	0	13.4 ± 0.2	9.02	9.86
L = $P(OMe)_3$, X = OMe (**16c**)	110	7	13.7 ± 0.1	8.88	9.79

Table 4
k_{obs} of C–H activation using 50 equivalents of aldehyde (20 ± 2 °C)

$[Cp^*(L)Rh(Me)(XC_6H_4CHO)]^+(\eta^1$-aldehyde adduct)	L = PMe_3 (**15**)	L = $P(OMe)_3$ (**16**)	Rate ratio (**15**/**16**)
X = CF_3 (**a**)	$5.4 \pm 0.4 \times 10^{-4}$ s^{-1}	$5.2 \pm 0.3 \times 10^{-5}$ s^{-1}	10
X = CH_3 (**b**)	$2.1 \pm 0.1 \times 10^{-4}$ s^{-1}	$1.2 \pm 0.4 \times 10^{-5}$ s^{-1}	18
X = OMe (**c**)	$9.0 \pm 0.5 \times 10^{-5}$ s^{-1}	$2.9 \pm 0.3 \times 10^{-6}$ s^{-1}	31

Table 5
$\Delta G^{\ddagger}$ for activation of aldehydic C–H bonds (20 ± 2 °C)

$[Cp^*(L)Rh(Me)(XC_6H_4CHO)]^+(\eta^1$-aldehyde adduct)	L = PMe_3 (**15**)	L = $P(OMe)_3$ (**16**)
X = CF_3 (**a**)	21.5 ± 0.1 kcal/mol	22.9 ± 0.1 kcal/mol
X = CH_3 (**b**)	22.1 ± 0.1 kcal/mol	23.7 ± 0.1 kcal/mol
X = OMe (**c**)	22.6 ± 0.2 kcal/mol	24.6 ± 0.1 kcal/mol

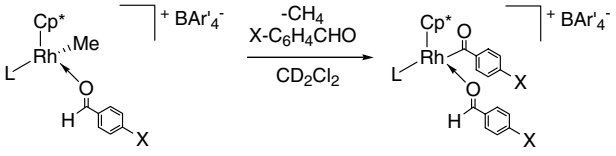

(5)

As noted earlier, C–H bond activation of benzene by **1** and **3** occurs at essentially equal rates. In these cases benzene is a weakly binding substrate and does not compete with CH_2Cl_2. That is, no benzene adduct is observed during the activation reaction. In the case of aryl aldehyde activation, the aldehyde adducts, **15a**–**15c** and **16a**–**16c**, rather than the CH_2Cl_2 adducts, are the more stable species, and as shown in Scheme 1, C–H bond activation is initiated from these species. The rates of C–H bond activation of these complexes correlate qualitatively with the rates of dissociation of the aldehydes. The more electron-rich PMe_3 complexes show higher rates of dissociation and higher rates of C–H bond activation than their $P(OMe)_3$ congeners. Similarly, the more electron-deficient aldehydes show faster rates of dissociation and higher rates of C–H bond activation (**15a** > **15b** > **15c**; **16a** > **16b** > **16c**). These rate trends can be rationalized by considering the expected substituent effects on the ground state aldehyde complexes relative to the transition state for C–H bond activation (Scheme 1). In the σ-aldehyde complexes there will be substantial partial positive charge on the carbonyl carbon due to polarization of the C=O π bond upon binding to the Lewis acidic Rh center. Ground state energies of these σ-complexes will be significantly affected by resonance and inductive effects of *para* substituents. In the four-centered transition state for C–H bond activation, Lewis acidic rhodium will no longer be bound exclusively to oxygen, thus *para*-substituent effects, especially π effects, should be less significant in affecting relative transition state energies. In short, electron-donating substituents will stabilize the aldehyde adducts **15** and **16** more than the corresponding transition states and thus retard the rate of C–H bond activation.

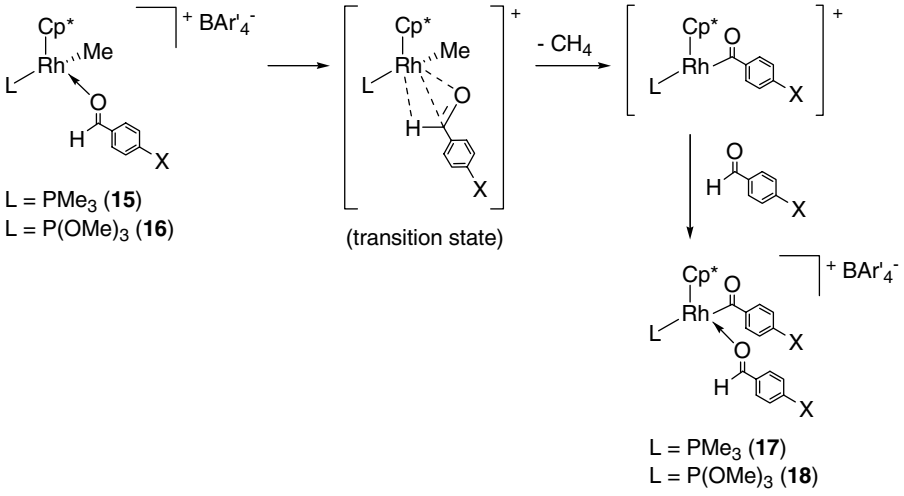

Scheme 1.

When 5 equivalents of tolualdehyde is allowed to undergo reaction with cationic Rh methyl complex **1** at room temperature, facile C–H bond activation and decarbonylation occurs, as evidenced by extrusion of methane and formation of $[Cp^*(PMe_3)Rh(C_6H_4CH_3)(CO)]BAr'_4$ (**19**). X-ray quality orange crystals of **19** were isolated via pentane layering of the reaction mixture. The ORTEP diagram is shown in Fig. 2, with some selected bond distances and bond angles listed in Table 6.

Contrary to the reaction described above between **1** and tolualdehyde, the reactions of Rh phosphite complex **3** with aryl aldehydes do not result in clean formation of decarbonylation products. A variety of species can be detected by ^1H and $^{31}P\{^1H\}$ NMR spectroscopy. The concentrations of these species fluctuate as a function of time, and vary with the particular aldehyde used along with the initial ratio of Rh complex to aldehyde. In the case of the reaction between **3** and tolualdehyde, several reaction products and intermediates have been identified by independent synthesis. Prior to proposing a sequence of reactions for the C–H activation and decarbonylation process, generation of potential intermediates is outlined below.

The ^{13}C-labeled Rh methyl carbonyl complex, $[Cp^*(P(OMe)_3)Rh(Me)(^{13}CO)]BAr'_4$ (**20′**), was readily generated in situ by exposure of a CD_2Cl_2 solution of **3** to ^{13}CO at 25 °C (Eq. (6)).

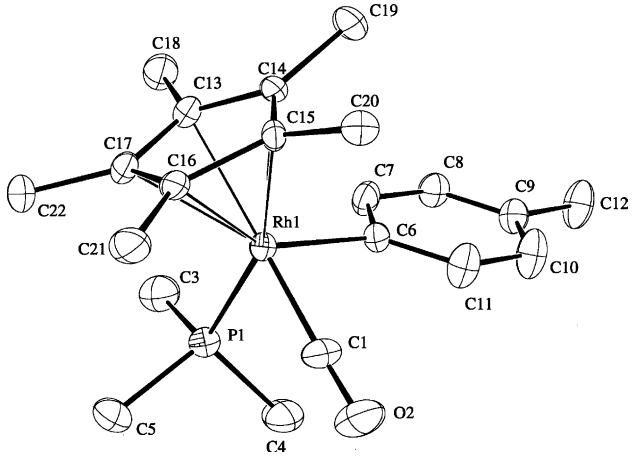

Fig. 2. ORTEP diagram of $[Cp^*(PMe_3)Rh(C_6H_4CH_3)(CO)]^+$ (**19**, BAr'^-_4 counterion omitted for clarity).

Table 6
Selected bond distances and bond angles for complex **19**

	Bond distance (Å)		Bond angle (°)
Rh(1)–C(16)	2.246(7)	C(16)–Rh(1)–P(1)	124.3(2)
Rh(1)–P(1)	2.298(3)	C(6)–Rh(1)–C(1)	89.4(3)
Rh(1)–C(6)	2.091(8)	P(1)–Rh(1)–C(6)	87.2(2)
Rh(1)–C(1)	1.879(8)	P(1)–Rh(1)–C(1)	89.0(3)
C(1)–O(2)	1.134(10)	Rh(1)–C(1)–O(2)	174.6(8)

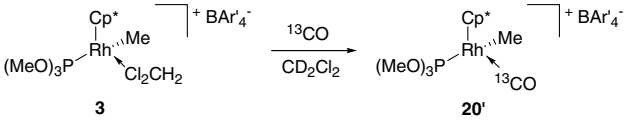

(6)

The corresponding ^{13}C-labeled Rh tolyl carbonyl complex, $[Cp^*(P(OMe)_3)Rh(C_6H_4CH_3)(^{13}CO)]BAr'_4$ (**21′**), was generated by an analogous reaction using $[Cp^*(P(OMe)_3)Rh(C_6H_4CH_3)(CH_2Cl_2)]BAr'_4$ (**22**), as shown in Scheme 2. The independent synthesis and characterization of **22** is detailed in Section 4. Interestingly, formation of **21′** by exposure of a CD_2Cl_2 solution of **22** to ^{13}CO was accompanied by formation of a rhodium acyl carbonyl complex (**23′**), which results from migratory insertion of carbon monoxide from **21′** followed by trapping with additional ^{13}CO (Scheme 2). Addition of excess $P(OMe)_3$ to a mixture of **21′** and **23′** led to the Rh bis-phosphite acyl complex $[Cp^*(P(OMe)_3)_2Rh(^{13}C(O)C_6H_4CH_3)]BAr'_4$ (**24′**). To generate Rh tolyl aldehyde adduct **25**, excess tolualdehyde was added to a CD_2Cl_2 solution of **22** (Scheme 2). NMR parameters for these species, which have been generated in situ, are summarized in Section 4.

Scheme 3 summarizes a proposed reaction sequence which accounts for the various species observed during the C–H activation and decarbonylation process involving cationic Rh methyl **3** and tolualdehyde. This reaction proceeds over the course of several days at room temperature, and was monitored by NMR spectroscopy.

As noted above, treatment of **3** with excess tolualdehyde (25–50 equivalents) results in immediate formation of Rh aldehyde adduct **16b**. After ca. 4 days, the C–H activation product, Rh acyl aldehyde **18b**, is formed as the major species (Scheme 3). Exchange of free aldehyde with bound aldehyde in **18b** is rapid at room temperature, but distinct aldehydic proton resonances for free and η^1-bound aldehyde could be observed by ^1H NMR spectroscopy at −88 °C. Treatment of **18b** with one equivalent of $P(OMe)_3$ results in complete conversion to the Rh bis-phosphite acyl complex $[Cp^*(P(OMe)_3)_2Rh(C(O)C_6H_4CH_3)]BAr'_4$ (**24**). In addition to the presence of **18b** as the major species, the Rh tolyl carbonyl complex $[Cp^*(P(OMe)_3)Rh(C_6H_4CH_3)(CO)]BAr'_4$ (**21**) and the Rh methyl carbonyl complex $[Cp^*(P(OMe)_3)Rh(Me)(CO)]BAr'_4$ (**20**) were also detected, along with small amounts of unidentified rhodium compounds (Scheme 3). Formation of **20** can be attributed to transfer of CO from **21** to either **3** (CO displaces coordinated dichloromethane) or **16b** (CO displaces coordinated aldehyde).

Treatment of **3** with 5 equivalents of tolualdehyde results in formation of **16b**, which decays predominantly to **20** and **21**. In this case we see very little build-up of

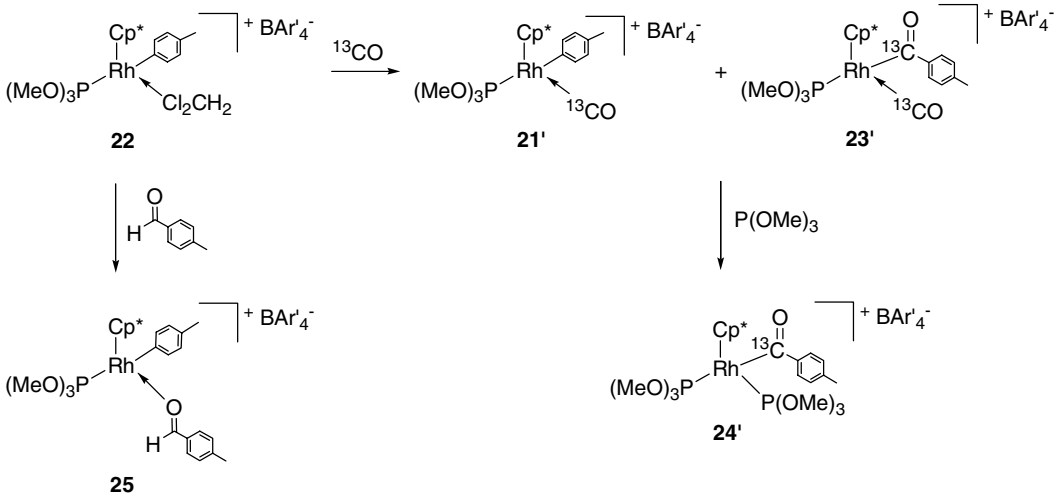

Scheme 2.

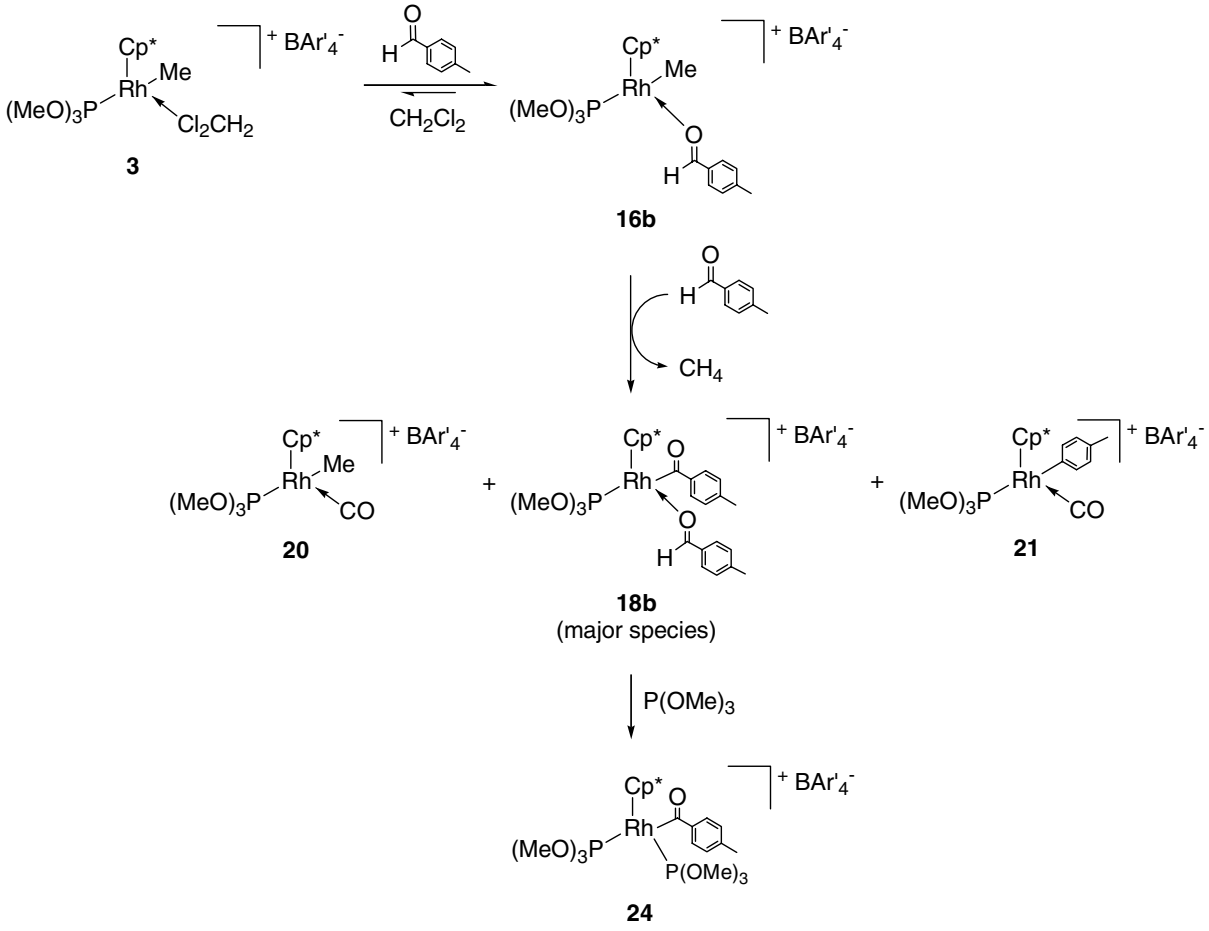

Scheme 3.

18b due to the low concentration of aldehyde present. After 16 days, the only identifiable product remaining is Rh methyl carbonyl **20**, which presumably, is the most stable species. When anisaldehyde or 4-(trifluoromethyl)benzaldehyde are used in the reaction with **3**, similar reactivity patterns emerge. However, the Rh acyl anisaldehyde adduct (the analogue of **18b**) is more stable than the Rh acyl tolualdehyde adduct (**18b**) due to the

tighter binding of the more basic anisaldehyde. The least basic aldehyde, 4-(trifluoromethyl)benzaldehyde, forms the least stable Rh acyl aldehyde adduct.

3. Conclusions

The work described here has provided new insights into the primary steps involved in C–H activation reactions that occur at cationic Group 9 M(III) centers. It has also revealed significant differences between the way such reactions take place at rhodium and iridium. Specifically, the focus on rhodium in this work has allowed us to measure the rates of exchange of free and bound aldehyde in the rhodium aldehyde complexes **15** and **16**. It has also revealed that in the presence of high concentrations of aldehyde, Rh acyl complexes, formed by decarbonylation of aryl aldehydes, can be stabilized by coordination of a second molecule of aldehyde, leading to cationic Rh acyl aldehyde complexes that are stable enough to be characterized in solution.

Our ability to observe the coordination and exchange of aldehyde at cationic Rh(III), and the subsequent C–H activation reaction, has allowed us to examine and compare the electronic effects on both processes. The factors that contribute to strong or weak aldehyde binding to the Rh^+ center appear to be dominated by σ-donation effects, as one would expect for a relatively electrophilic metal center. The rates of exchange and C–H activation are strongly correlated. The primary influence on the overall C–H activation rate is a ground state effect: when the aldehyde is strongly bound to the Rh^+ center, this binding retards its rearrangement to the transition state for C–H activation. Conversely, a more loosely-held aldehyde rearranges more easily to the transition state, facilitating the C–H activation process. Thus this system reflects a property often noted for enzymes: strong coordination of substrate to an active site does not necessarily promote efficient catalysis, and in fact can have the opposite effect [13]. The optimum situation for catalysis involves relatively weak binding of substrate in the ground state, so that this interaction does not counteract the binding energy of the rearranging substrate to the active site in the transition state.

4. Experimental

4.1. General considerations

Unless otherwise noted, all reactions and manipulations were performed using standard high-vacuum, Schlenk, or drybox techniques. Argon and nitrogen were purified by passage through columns of BASF R3-11 catalyst (Chemalog) and 4 Å molecular sieves. ^1H and ^{13}C NMR chemical shifts were referenced to residual ^1H and ^{13}C NMR signals of the deuterated solvents, respectively. ^{31}P NMR chemical shifts were referenced to an 85% H_3PO_4 sample used as an external standard. Elemental analyses were performed by Atlantic Microlab Inc. of Norcross, GA.

4.2. Materials

All solvents were deoxygenated and dried via passage over a column of activated alumina [14]. Deuterated solvents (Cambridge Isotope Laboratories) were purified by vacuum transfer from CaH_2 and stored over 4 Å molecular sieves. Unless otherwise noted, all chemicals were purchased from Aldrich and used without further purification. ^{13}C-labeled CO was purchased from Cambridge Isotope Laboratories. $NaBAr'_4$ was purchased from Boulder Scientific and used without further purification. Solutions of 1.5 M MeLi and PhLi in Et_2O were purchased from Acros and used without further purification. Organometallic complexes **1** [8], **2** [15], Cp*(P(OMe)$_3$)$RhCl_2$ [9], and Cp*(PMe_3)Rh(Ph)(Cl) [11] have been previously reported and were synthesized according to literature procedures.

4.3. Spectral data for BAr'^-_4

The ^1H and ^{13}C NMR resonances of the BAr'_4 (Ar′ = 3,5-$(CF_3)_2C_6H_3$) counteranion in CD_2Cl_2 were essentially invariant for all cationic complexes discussed here and spectroscopic data are not repeated for each compound. ^1H NMR (400 MHz, CD_2Cl_2) δ 7.73 (s, 8 H, H_{ortho}), 7.57 (s, 4 H, H_{para}). $^{13}C\{^1H\}$ NMR (101 MHz, CD_2Cl_2) δ 161.9 (q, $^1J_{C-B} = 49.8$, C_{ipso}), 135.0 (s, C_{ortho}), 129.0 (q, $^2J_{C-F} = 31.4$, C_{meta}), 124.7 (q, $^1J_{C-F} = 272.6$, CF_3), 117.7 (s, C_{para}).

4.4. Synthesis of $[Cp^*(P(OMe)_3)Rh(Me)(CH_2Cl_2)]BAr'_4$ (**3**)

A vial was charged with 172 mg (0.412 mmol) of **4** and 408 mg (0.461 mmol) of $NaBAr'_4$. The reactants were dissolved in 5 mL of CH_2Cl_2 and the resulting mixture was stirred for 5 min. The contents were filtered and stored at −35 °C for 24 h. Red–orange crystals of **3** were isolated in 55% yield. ^1H NMR (300 MHz, CD_2Cl_2) δ 5.33 (s, CH_2Cl_2), 3.78 (d, $^3J_{P-H} = 11.4$ Hz, 9 H, P(OMe)$_3$), 1.63 (d, $^4J_{P-H} = 4.2$ Hz, 15 H, Cp*), 1.02 (dd, $^3J_{P-H} = 5.5$ Hz, $^2J_{Rh-H} = 1.5$ Hz, 3 H, Me). $^{31}P\{^1H\}$ NMR (121.5 MHz, CD_2Cl_2) δ 126.9 (d, $^1J_{Rh-P} = 268.6$ Hz, P(OMe)$_3$). $^{13}C\{^1H\}$ NMR (101 MHz, CD_2Cl_2) δ 103.3 (s, Cp*–Ar), 54.34 (d, $^2J_{P-C} = 8.0$ Hz, P(OMe)$_3$), 54.19 (s, CH_2Cl_2), 9.16 (d, $^3J_{P-C} = 1.4$ Hz, Cp*–Me), 1.19 (dd, $^2J_{P-C} = 37.1$ Hz, $^1J_{Rh-C} = 22.0$ Hz, Me).

4.5. Synthesis of $Cp^*(P(OMe)_3)Rh(Me)(Cl)$ (**4**)

To a flame-dried Schlenk flask under argon, 2.5 g (6.9 mmol) of $Cp^*(P(OMe)_3)RhCl_2$ was dissolved in 100 mL dry ether. The solution was cooled to −78 °C and methyllithium (7.6 mmol in THF) was added to the solution, which was then brought to room temperature. The reaction was opened to air and quenched with 10 mL of water, the ether phase was removed, and the red/orange product isolated by roto-evaporation. The crude product was dissolved in 20 mL CH_2Cl_2 to which hexanes were added (50 mL) until the solution became cloudy. Red–orange crystals were isolated in 50% yield. ^1H NMR (300 MHz, CD_2Cl_2) δ 3.68 (d, $^3J_{P-H}$ = 11.4 Hz, 9 H, $P(OMe)_3$), 1.61 (d, $^4J_{P-H}$ = 4.1 Hz, 15 H, Cp*), 0.73 (dd, $^3J_{P-H}$ = 5.1 Hz, $^2J_{Rh-H}$ = 2.1 Hz, 3 H, Me). $^{31}P\{^1H\}$ NMR (121.5 MHz, CD_2Cl_2) δ 138.36 (d, $^1J_{Rh-P}$ = 259.9 Hz, $P(OMe)_3$). $^{13}C\{^1H\}$ NMR (101 MHz, CD_2Cl_2) δ 100.00 (vt, $^1J_{Rh-C} = {}^2J_{P-C}$ = 4. 2 Hz, Cp*–Ar), 53.00 (d, $^2J_{P-C}$ = 4.38 Hz, $P(OMe)_3$), 8.94 (d, J = 2.25 Hz, Cp*–Me), −2.57 (dd, $^1J_{Rh-C}$ = 22.2 Hz $^2J_{P-C}$ = 20.6 Hz, Me).

4.6. Synthesis of $[Cp^*(PMe_3)Rh(Ph)(CH_2Cl_2)]BAr'_4$ (**6**)

A Schlenk flask was charged with 50 mg (0.117 mmol) of $Cp^*(PMe_3)Rh(Ph)(Cl)$ and 109 mg (0.123 mmol) of $NaBAr'_4$ and sealed with a rubber stopper. The flask was placed in an ice bath and 5 mL of CH_2Cl_2 was introduced via syringe. The contents of the flask were stirred for 5 min and then filtered through Celite supported by a glass frit. The filtrate was concentrated in vacuo and the flask placed in a freezer (−30 °C) for 3 d. Orange–red crystals of **6** (110 mg, 0.082 mmol) were isolated in 70% yield and can be stored at −30 °C for weeks. ^1H NMR (400 MHz, CD_2Cl_2, 0 °C) δ 7.19 (br m, 2 H, Ph), 7.07 (br m, 3 H, Ph), 5.33 (s, CH_2Cl_2), 1.51 (d, $^4J_{P-H}$ = 2.7 Hz, 15 H, Cp*), 1.46 (d, $^2J_{P-H}$ = 10.1 Hz, 9 H, PMe_3). $^{31}P\{^1H\}$ NMR (162 MHz, CD_2Cl_2, 0 °C) δ 1.1 (d, $^1J_{Rh-P}$ = 168.2 Hz, PMe_3). $^{13}C\{^1H\}$ NMR (101 MHz, CD_2Cl_2, 0 °C) δ 158.3 (dd, $^1J_{Rh-C}$ = 32.0 Hz, $^2J_{P-C}$ = 17.5 Hz, Ph–C_{ipso}), 136.2 (d, $^2J_{Rh-C}$ = 4.6 Hz, Ph–C_{ortho}), 130.2 (s, Ph–C_{meta}), 125.1 (s, Ph–C_{para}), 103.1 (s, Cp*–Ar), 54.1 (s, CH_2Cl_2), 15.31 (d, $^1J_{P-C}$ = 32.0 Hz, PMe_3), 9.66 (s, Cp*–Me).

4.7. Synthesis of $[Cp^*(P(OMe)_3)Rh(Ph)(CH_2Cl_2)]BAr'_4$ (**7**)

In a J-Young NMR tube, 15.9 mg (0.01 mmol) of **3** was dissolved in 0.5 mL of 1.1 M benzene in CD_2Cl_2. After 24 h, the volatile materials were removed to yield a light orange powder in quantitative yields. ^1H NMR (400 MHz, CD_2Cl_2) δ 7.30 (m, 5 H, Ph), 3.74 (d, $^3J_{P-H}$ = 11.2 Hz, 9 H, $P(OMe)_3$), 1.56 (d, $^4J_{P-H}$ = 4.4 Hz, 15 H, Cp*). $^{31}P\{^1H\}$ NMR (162 MHz, CD_2Cl_2) δ 121.7 Hz (d, $^1J_{Rh-P}$ = 268.4 Hz, $P(OMe)_3$).

4.8. Generation of $[Cp^*(P(OMe)_3)Rh(Me)(p\text{-}CH_3C_6H_4CHO)]BAr'_4$ (**16b**)

In a J-Young NMR tube 15.0 mg (0.01 mmol) of **3** was dissolved in 0.5 mL CD_2Cl_2, and tolualdehyde (5 equivalents, 6.0 μL, 0.055 mmol) was added to the solution. At −68 °C, **16b** and the aldehydic protons of both the bound and free aldehyde were observable by NMR spectroscopy. ^1H NMR (300 MHz, CD_2Cl_2, −68 °C) δ 9.11 (s, 1 H, $CH_3C_6H_4CO$-*H*), 3.69 (d, $^3J_{P-H}$ = 11.7 Hz, 9 H, $P(OMe)_3$), 1.64 (d, $^4J_{P-H}$ = 4.2 Hz, 15 H, Cp*), 0.96 (dd, $^3J_{P-H}$ = 5.4 Hz, $^2J_{Rh-H}$ = 1.6 Hz, 3 H, Me). $^{31}P\{^1H\}$ NMR (121.5 MHz, CD_2Cl_2, −68 °C) δ 132.1 Hz (d, $^1J_{Rh-P}$ = 266 Hz, $P(OMe)_3$).

4.9. Generation of $[Cp^*(P(OMe)_3)Rh(C(O)C_6H_4CH_3)(p\text{-}CH_3C_6H_4CHO)]BAr'_4$ (**18b**)

In a J-Young NMR tube 15.0 mg (0.01 mmol) of **3** was dissolved in 0.5 mL CD_2Cl_2 and 50 μL of tolualdehyde was added to the solution. After 3 days, the solution was cooled to −68 °C to allow for the resolution (by NMR spectroscopy) of the aldehydic proton of bound aldehyde in **18b**.^1H NMR (300 MHz, CD_2Cl_2, −68 °C) δ 9.58 (s, 1 H, $CH_3C_6H_4CO$–*H*), 3.81 (d, $^3J_{P-H}$ = 11.1 Hz, 9 H, $P(OMe)_3$), 1.71 (d, $^4J_{P-H}$ = 5.3 Hz, 15 H, Cp*). $^{31}P\{^1H\}$ NMR (121.5 MHz, CD_2Cl_2, −68 °C) δ 115.4 Hz (d, $^1J_{Rh-P}$ = 235 Hz, $P(OMe)_3$).

4.10. Synthesis of $[Cp^*(PMe_3)Rh(C_6H_4CH_3)(CO)]BAr'_4$ (**19**)

A Schlenk flask was charged with 30 mg (0.023 mmol) of **1** and 1 mL of dichloromethane. A dichloromethane solution of tolualdehyde (0.115 mmol) was added via syringe and the contents of the flask were allowed to stir overnight. To afford crystals, 1 mL of pentane was added and the flask placed in a freezer at −30 °C. After 6 d, 12 mg (0.0093 mmol) of X-ray quality orange crystals were isolated in 39% yield. ^1H NMR (400 MHz, CD_2Cl_2) δ 6.99 (d, ^3J = 7.7 Hz, 2 H, tolyl-Ar), 6.91 (d, $^3J_{H-H}$ = 7.7 Hz, 2 H, tolyl-Ar), 2.28 (s, 3 H, tolyl-Me), 1.84 (d, $^4J_{P-H}$ = 2.9 Hz, 15 H, Cp*), 1.50 (d, $^2J_{P-H}$ = 10.8 Hz, 9 H, PMe_3). $^{31}P\{^1H\}$ NMR (162 MHz, CD_2Cl_2) δ 4.1 (d, $^1J_{Rh-P}$ = 129.1 Hz, PMe_3). $^{13}C\{^1H\}$ NMR (101 MHz, CD_2Cl_2) δ 188.8 (dd, $^1J_{Rh-C}$ = 72.5 Hz, $^2J_{P-C}$ = 21.9 Hz, CO), 138.5 (br m, C_{ipso} of tolyl-Ar), 136.0 (s, tolyl-Ar), 131.9 (s, tolyl-Ar), 130.1 (s, tolyl-Ar), 107.6 (s, Cp*–Ar), 20.59 (s, tolyl-Me), 16.43 (d, $^1J_{P-C}$ = 35.6 Hz, PMe_3), 9.89 (s, Cp*–Me). *Anal.* Calc. for $C_{53}H_{43}OBF_{24}PRh$: C, 49.10; H, 3.34. Found: C, 48.93; H, 3.12%.

4.11. Synthesis of $[Cp^*(P(OMe)_3)Rh(p\text{-}C_6H_4CH_3)(CH_2Cl_2)]BAr'_4$ (**22**)

In the glove box, a vial was charged with 36 mg (0.075 mmol) of $Cp^*(P(OMe)_3)Rh(C_6H_4\ CH_3)(Cl)$ (see below for synthesis of this compound) and 72 mg (0.081 mmol) of $NaBAr'_4$. The reactants were dissolved in 2 mL of CH_2Cl_2. The contents were filtered and stored at −35 °C for 24 h. An orange powder was isolated in 40% yield. ^1H NMR (300 MHz, CD_2Cl_2) δ 6.95 (d, $J = 8.1$ Hz, 2 H, tolyl-H), 7.26 (d, J = 7.2 Hz, 2 H, tolyl-H), 3.68 (d, $^3J_{P-H} = 10.8$ Hz, 9 H, $P(OMe)_3$), 2.24 (s, 3 H, tolyl-CH_3), 1.48 (d, $^4J_{P-H} = 4.5$ Hz, 15 H, Cp*). $^{31}P\{^1H\}$ NMR (121.5 MHz, CD_2Cl_2) δ 126.8 Hz (d, $^1J_{Rh-P} = 260$ Hz, $P(OMe)_3$). $^{13}C\{^1H\}$ NMR (75.5 MHz, CD_2Cl_2) δ 131.1 (s, tolyl-Ar) 102.6 (s, Cp*–Ar), 54.72 (d, $^2J_{P-C} = 7.6$ Hz, $P(OMe)_3$), 20.44 (s, tolyl-Me), 8.71 (s, Cp*–Me).

4.12. Synthesis of $Cp^*(P(OMe)_3)Rh(C_6H_4CH_3)(Cl)$

To a flame dried Schlenk flask under argon, $Cp^*(P(OMe)_3)RhCl_2$ was dissolved in 40 mL dry THF and the resulting solution was cooled to −78 °C. Tolyl-lithium (2.3 equivalents, 321 mg, 3.28 mmol) [16] was dissolved in 10 mL of THF, and the resulting solution was cooled to −78 °C and cannula-transferred into a stirred solution of $Cp^*(P(OMe)_3)RhCl_2$ at which point the color changed from red to orange. After being brought to room temperature the solvent was removed to yield an orange foam, which was then extracted with 3×20 mL toluene and filtered through celite. Concentration of this solution under vacuum yielded a red oil which, upon addition of pentane and cooling to −78 °C afforded an orange powder in 46% yield. ^1H NMR (300 MHz, CD_2Cl_2) δ 7.36 (d, $J = 7.2$ Hz, tolyl-H), 6.80 (d, $J = 7.6$ Hz, tolyl-H), 3.49 (d, $^3J_{P-H} = 11.4$ Hz, 9 H, $P(OMe)_3$), 2.22 (s, tolyl-Me), 1.50 (d, $^4J_{P-H} = 4.1$ Hz, 15 H, Cp*), $^{31}P\{^1H\}$ NMR (121.5 MHz, CD_2Cl_2) δ 135.56 (d, $^1J_{Rh-P} = 247.0$ Hz, $P(OMe)_3$). $^{13}C\{^1H\}$ NMR (101 MHz, CD_2Cl_2) δ 139.41 (s, tolyl-Ar), 131.97 (s, tolyl-Ar), 128.93 (s, tolyl-Ar), 101.60 (d, $J = 4.6$ Hz, Cp*–Ar), 53.66 (d, $^3J_{P-C} = 4.6$ Hz, $P(OMe)_3$), 21.14 (s, tolyl-*C* H_3), 9.29 (d, $J = 1.61$ Hz, Cp*–Me).

4.13. Synthesis of $[Cp^*(P(OMe)_3)Rh(C_6H_4CH_3)(p\text{-}CH_3C_6H_4CHO)]\ BAr'_4$ (**25**)

In a J-Young NMR tube 15.0 mg (0.010 mmol) of **22** was dissolved in 0.5 mL CD_2Cl_2 and 25 μL of tolualdehyde was added to the solution. The solution was cooled to −68 °C to allow for the resolution of the aldehydic proton of bound aldehyde. ^1H NMR (300 MHz, CD_2Cl_2, −68 °C) δ 8.98 (s, *p*-$CH_3C_6H_4CO$-*H*), 6.95 (d, J = 7.7 Hz, 2 H, tolyl-H), 7.26 (d, partially obscured, 2 H, *m*-Ar–H), 3.68 (d, $^3J_{P-H} = 10.8$ Hz, 9 H, $P(OMe)_3$), 2.13 (s, 3 H, tolyl-CH_3), 1.50 (d, $^4J_{P-H} = 4.5$ Hz, 15 H, Cp*). $^{31}P\{^1H\}$ NMR (121.5 MHz, CD_2Cl_2, −68 °C) δ 126.8 Hz (d, $^1J_{Rh-P} = 260$ Hz, $P(OMe)_3$).

4.14. Generation of $[Cp^*(P(OMe)_3)Rh(Me)(^{13}CO)]BAr'_4$ (**20′**)

In a J-Young NMR tube 15.0 mg (0.011 mmol) of **3** was dissolved in 0.5 mL CD_2Cl_2. The solution was subject to three freeze–pump–thaw cycles, at which point the headspace of the tube was backfilled with ^{13}CO. Upon shaking of the tube, the solution turned from orange to light yellow. ^1H and ^{31}P NMR spectroscopy showed complete conversion of **3** to **20′**. ^1H NMR (300 MHz, CD_2Cl_2) δ 3.77 (d, $^3J_{P-H} = 12.0$ Hz, 9 H, $P(OMe)_3$), 1.87 (d, $^4J_{P-H} = 4.8$ Hz, 15 H, Cp*), 0.78 (dd, $^3J_{P-H} = 3.9$ Hz, $^2J_{Rh-H} = 2.1$ Hz, 3 H, Me). $^{31}P\{^1H\}$ NMR (121.5 MHz, CD_2Cl_2) δ 121.6 Hz (d, $^1J_{Rh-P} = 217$ Hz, $P(OMe)_3$). $^{13}C\{^1H\}$ NMR (101 MHz, CD_2Cl_2) δ 187.1 (dd, $^1J_{Rh-C} = 70.7$ Hz, $^2J_{P-C} = 32.0$ Hz, ^{13}CO).

4.15. Generation of $[Cp^*(P(OMe)_3)Rh(C_6H_4CH_3)(^{13}CO)]BAr'_4$ (**21′**)

A J-Young tube with 35 mg of **22** in 0.5 mL CD_2Cl_2 was freeze–pump-thawed three times and backfilled with ^{13}CO. The solution was shaken, and excess ^{13}CO was evacuated from the headspace and backfilled with argon while the solution was frozen. ^1H, ^{13}C and ^{31}P NMR spectroscopy showed the presence of both **21′** and **23′** (see below) in solution. ^1H NMR (300 MHz, CD_2Cl_2) δ 6.98 (d, $J = 7.8$ Hz, 2 H, tolyl-H), 7.05 (d, J = 7.8 Hz, 2 H, tolyl-H), 3.63 (d, $^3J_{P-H} = 12.0$ Hz, 9 H, $P(OMe)_3$), 2.25 (s, 3 H, tolyl-CH_3), 1.77 (d, $^4J_{P-H} = 4.8$ Hz, 15 H, Cp*). $^{31}P\{^1H\}$ NMR (121.5 MHz, CD_2Cl_2) δ 116.9 Hz (dd, $^1J_{Rh-P} = 215$ Hz, $^2J_{P-C} = 32.8$ Hz, $P(OMe)_3$). $^{13}C\{^1H\}$ NMR (101 MHz, CD_2Cl_2) δ 187.5 (dd, $^1J_{Rh-C} = 68.3$ Hz, $^2J_{P-C} = 38.4$ Hz, ^{13}CO).

4.16. Generation of $[Cp^*(P(OMe)_3)Rh(^{13}C(O)\text{-}C_6H_4CH_3)(^{13}CO)]BAr'_4$ (**23′**)

A J-Young tube charged with 35 mg of **22** in 0.5 mL CD_2Cl_2. The contents were freeze–pump-thawed three times and backfilled with ^{13}CO. The solution was shaken, and excess ^{13}CO was evacuated from the headspace and backfilled with argon while the solution was frozen. ^1H, ^{13}C and ^{31}P NMR spectroscopy showed the presence of both **21′** and **23′** in solution. ^1H NMR (300 MHz, CD_2Cl_2) δ 7.31 (m, 4 H, Ar–H), 3.74 (d, $^3J_{P-H} = 11.7$ Hz, 9 H, $P(OMe)_3$), 2.39 (s, 3 H, tolyl-CH_3), 1.88 (d, $^4J_{P-H} = 3.9$ Hz, 15 H, Cp*). $^{31}P\{^1H\}$ NMR (121.5 MHz, CD_2Cl_2) δ 114.7 (ddd, $^1J_{Rh-P} = 226$ Hz, $^2J_{P-C} = 35.2$ Hz, $^2J_{P-C} = 12.1$ Hz, $P(OMe)_3$). $^{13}C\{^1H\}$ NMR (101 MHz, CD_2Cl_2) δ 223.6 (ddd, $^1J_{Rh-C} =$

23.3 Hz, $^{2}J_{P-C}$ = 10.9,$^{2}J_{C-C}$ = 3.0 Hz, Rh–acyl-^{13}CO), 188.5 (ddd, $^{1}J_{Rh-C}$ = 74.7 Hz, $^{2}J_{P-C}$ = 34.8Hz,$^{2}J_{C-C}$ = 3.0 Hz, Rh–^{13}CO).

4.17. Generation of [Cp*(P(OMe)$_3$)$_2$Rh(^{13}C(O)C$_6$H$_4$CH$_3$)]BAr′$_4$ (24′)

A J-Young tube containing a mixture of **21′** and **23′** in CD_2Cl_2 solution (product from synthesis of **21′**) was brought into the glove box where 3.1 μL of trimethyl phosphite was introduced. After 1 day at room temperature, the resulting yellow solution was decanted from precipitate, at which point **24′** was the only species detected in solution. Alternatively, **24′** can be generated by the addition of trimethyl phosphite to a solution of **18b**. ^{1}H NMR (300 MHz, CD_2Cl_2) δ 7.35 (m, 2 H, tolyl-H$_{ortho}$), 7.19 (d, J = 8.1 Hz, 2 H, tolyl-H$_{meta}$), 3.72 (t, J = 5.7 Hz, 18 H, P(OMe)$_3$), 2.39 (s, 3 H, tolyl-CH$_3$), 1.66 (t, $^{4}J_{P-H}$ = 4.6 Hz, 15 H, Cp*). ^{31}P{^{1}H} NMR (121.5 MHz, CD_2Cl_2) δ 119.1 (dd, $^{1}J_{Rh-P}$ = 244 Hz, $^{2}J_{P-C}$ = 11.9 Hz, P(OMe)$_3$). ^{13}C{^{1}H} NMR (75.5 MHz, CD_2Cl_2) δ 233.21 (dt, $^{1}J_{Rh-C}$ = 29.1 Hz, $^{2}J_{P-C}$ = 12.2 Hz, Rh–^{13}*C*O-tolyl), 142.90 (s, tolyl-Ar), 128.8 (br d, tolyl-Ar), 128.5 (br d, tolyl-Ar), 125.1 (s, tolyl-Ar), 106.1 (m, Cp*–Ar), 55.17 (m, P(OMe)$_3$), 21.27 (tolyl-Me), 9.67 (s, Cp*–Me).

4.18. Kinetics of C–H activation reactions of aldehydes using 1 and 3

Reactions using 10–20 mg of **1** or **3** (0.03 M) with aldehydes (1.5 M) were carried out in J-Young NMR tubes in CD_2Cl_2. Values of k_{obs} were determined by integration of the rhodium–methyl and Cp* peaks relative to the invariant BAr'_4 peaks during reaction of **1** and **3** with 50 equivalents of aldehyde over the course of days at room temperature.

4.19. Determination of $\Delta G^{\ddagger}$ for dissociative exchange of aldehydes in 15 and 16

Solutions of 10 mg of **1** or **3** in CD_2Cl_2 were combined with 5 equivalents of aldehyde and cooled to −88 °C. At this temperature, the natural $w_{1/2}$ of the aldehydic proton was determined. The $w_{1/2}$ was again measured at a temperature where the width had reached 5–10 times the natural line width. Rate constants for exchange and $\Delta G^{\ddagger}$ were calculated from this data using the slow exchange equation $k = \pi(\Delta w)$.

4.20. Crystallographic studies

For complexes **6** and **19**, data were collected at −100 °C on a Bruker SMART diffractometer, using the omega scan mode. Crystal data and collection parameters are given in Table 7. All computations were performed using the NRCVAX suite of programs [17].

Table 7
Crystallographic data and collection parameters for **6** and **19**

	6	19
Empirical formula	$RhPC_{52}H_{43}BF_{24}Cl_2$	$RhPBC_{53}H_{43}F_{24}O$
Formula weight	1339.46	1317.79
Crystal system	monoclinic	triclinic
Space group	$P2_1/c$	$P\bar{1}$
a (Å)	12.5934(22)	12.3960(5)
b (Å)	18.824(3)	12.7232(6)
c (Å)	24.160(4)	18.3440(8)
α (°)	–	76.5570(10)
β (°)	94.260(7)	86.1510(10)
γ (°)	–	84.6820(10)
V (Å^3)	5711.3(15)	2798.67(21)
Z	4	2
D_{calc} (Mg/m^3)	1.558	1.564
Radiation	Mo Kα	Mo Kα
μ (mm^{-1})	0.53	0.47
R_f	0.129	0.098
R_w	0.131	0.086
Goodness-of-fit	1.8114	2.1963

5. Supplementary material

CCDC-240673 (**6**) and -240674 (**19**) contain the supplementary crystallographic data for this paper. These data can be obtained free of charge via www.ccdc.cam.ac.uk/data_request/cif, by emailing data_request@ccdc.cam.ac.uk, or by contacting The Cambridge Crystallographic Data Centre, 12, Union Road, Cambridge CB2 1EZ, UK; fax: +44 1223 336033.

Acknowledgement

B.K.C., F.L.T., and M.B. acknowledge the National Science Foundation (CHE-0107810) for support of this work and R.G.B. acknowledges support by the Director, Office of Energy Research, Office of Basic Energy Sciences, Chemical Sciences Division, of the US Department of Energy under Contract No. DE-AC03-7600098.

References

[1] (a) N.F. Gol'dshleger, V.V. Es'kova, A.E. Shilov, A.A. Shteinman, Zh. Fiz. Khim. 46 (1972) 1353;
(b) A.E. Shilov, A.A. Shteinman, Coord. Chem. Rev. 24 (1977) 97.
[2] (a) R.H. Crabtree, J.M. Mihelcic, J.M. Quirk, J. Am. Chem. Soc. 101 (1979) 7738;
(b) R.H. Crabtree, M.F. Mellea, J.M. Mihelcic, J.M. Quirk, J. Am. Chem. Soc. 104 (1982) 107;
(c) R.H. Crabtree, C.P. Parnell, Organometallics 4 (1985) 519;
(d) M.J. Burk, R.H. Crabtree, D.V. McGrath, J. Chem. Soc., Chem. Commun. 24 (1985) 1829;
(e) M.J. Burk, R.H. Crabtree, J. Am. Chem. Soc. 109 (1987) 8025.
[3] (a) D. Baudry, M. Ephritikhine, H. Felkin, R. Holmes-Smith, J. Chem. Soc., Chem. Commun. 14 (1983) 788;
(b) D. Baudry, M. Ephritikhine, H. Felkin, J. Zakrzewski, Tetrahedron Lett. 25 (1984) 1283;

(c) N. Aktogu, D. Baudry, D. Cox, M. Ephritikhine, H. Felkin, R. Holmes-Smith, J. Zakrzewski, Bull. Soc. Chim. Fr. 3 (1985) 381.
[4] (a) P. Burger, R.G. Bergman, J. Am. Chem. Soc. 115 (1993) 10462;
(b) B.A. Arndtsen, R.G. Bergman, Science 270 (1995) 1970.
[5] (a) R.L. Brainard, W.R. Nutt, T.R. Lee, G.M. Whitesides, Organometallics 7 (1988) 2379;
(b) S.S. Stahl, J.A. Labinger, J.E. Bercaw, J. Am. Chem. Soc. 118 (1996) 5961;
(c) M.W. Holtcamp, J.A. Labinger, J.E. Bercaw, J. Am. Chem. Soc. 119 (1997) 848;
(d) D.D. Wick, K.I. Goldberg, J. Am. Chem. Soc. 119 (1997) 10235;
(e) U. Fekl, K.I. Goldberg, Adv. Inorg. Chem. 54 (2003) 259, and references therein.
[6] (a) P.J. Alaimo, R.G. Bergman, Organometallics 18 (1999) 2707, and references therein;
(b) S.R. Klei, T.D. Tilley, R.G. Bergman, J. Am. Chem. Soc. 122 (2000) 1816.
[7] (a) A.H. Janowicz, R.G. Bergman, J. Am. Chem. Soc. 104 (1982) 352;
(b) J.K. Hoyano, W.A.G. Graham, J. Am. Chem. Soc. 104 (1982) 3723;
(c) W.D. Jones, F.J. Feher, J. Am. Chem. Soc. 104 (1982) 4240;
(d) A.A. Bengali, B.A. Arndtsen, P.M. Burger, R.H. Schultz, B.H. Weiller, K.R. Kyle, C.B. Moore, R.G. Bergman, Pure Appl. Chem. 67 (1995) 281.
[8] F.L. Taw, H. Mellows, P.S. White, F.J. Hollander, R.G. Bergman, M. Brookhart, D.M. Heinekey, J. Am. Chem. Soc. 124 (2002) 5100.
[9] P. Jutzi, M. Söte, B. Neumann, H.G. Stammler, J. Organomet. Chem. 556 (1998) 97.
[10] D.M. Tellers, C.M. Yung, B.A. Arndtsen, D.R. Adamson, R.G. Bergman, J. Am. Chem. Soc. 124 (2002) 1400.
[11] W.D. Jones, F.J. Feher, Inorg. Chem. 23 (1984) 2376.
[12] (a) P.J. Alaimo, B.A. Arndtsen, R.G. Bergman, J. Am. Chem. Soc. 119 (1997) 5269;
(b) P.J. Alaimo, B.A. Arndtsen, R.G. Bergman, Organometallics 19 (2000) 2130.
[13] A. Fersht, Enzyme Structure and Mechanism, 2nd ed., W.H. Freeman, New York, 1985.
[14] (a) A.B. Pangborn, M.A. Giardello, R.H. Grubbs, R.K. Rosen, F.J. Timmers, Organometallics 15 (1996) 1518;
(b) P.J. Alaimo, D.W. Peters, J. Arnold, R.G. Bergman, J. Chem. Educ. 78 (2001) 64.
[15] W.D. Jones, F.J. Feher, Organometallics 2 (1983) 562.
[16] M.P.R. Spee, J. Boersma, M.D. Meijer, M.Q. Slagt, G. van Koten, J.W. Geus, J. Org. Chem. 66 (2001) 1647.
[17] E.J. Gabe, Y. Le Page, J.P. Charland, F.L. Lee, P.S. White, J. Appl. Cryst. 22 (1989) 384.